NORTH-HOLLAND
PHYSICS
PUBLISHING

X-ray diffraction and continuous small-angle scattering of turkey tendons with the improved area detector at Frascati

Jitendra Shantilal Shah
H.H. Wills Physics Laboratory, University of Bristol, Bristol BS8 1TL, UK

Andrea La Monaca
INFN, Laboratori Nazionali di Frascati, PO Box 13, 00044 Frascati, Italy

Adriana Bigi and Norberto Roveri
Dipartimento di Chimica "G. Ciamician", via Selmi 2, University of Bologna, Italy

Low-angle diffraction experiments with turkey tendons were carried out with the Frascati drift-chamber area detector and diffraction camera. A fast CAMAC–VME–Macintosh IIx data acquisition system provided real-time graphics for monitoring and interpreting scattering and diffraction data. Results obtained on uncalcified turkey tendons show unfolding of crimps with tensile stretching. These results confirm the significance of crimps with respect to in vivo mechanical functions of these tissues. Results of continuous small-angle scattering in calcified turkey tendons and other substances are interpreted in terms of their structural anisotropy.

Reprinted from NUCLEAR INSTRUMENTS AND METHODS
IN PHYSICS RESEARCH A

Nuclear Instruments and Methods in Physics Research A308 (1991) 285–290
North-Holland

X-ray diffraction and continuous small-angle scattering of turkey tendons with the improved area detector at Frascati

Jitendra Shantilal Shah
H.H. Wills Physics Laboratory, University of Bristol, Bristol BS8 1TL, UK

Andrea La Monaca
INFN, Laboratori Nazionali di Frascati, PO Box 13, 00044 Frascati, Italy

Adriana Bigi and Norberto Roveri
Dipartimento di Chimica "G. Ciamician", via Selmi 2, University of Bologna, Italy

Low-angle diffraction experiments with turkey tendons were carried out with the Frascati drift-chamber area detector and diffraction camera. A fast CAMAC–VME–Macintosh IIx data acquisition system provided real-time graphics for monitoring and interpreting scattering and diffraction data. Results obtained on uncalcified turkey tendons show unfolding of crimps with tensile stretching. These results confirm the significance of crimps with respect to in vivo mechanical functions of these tissues. Results of continuous small-angle scattering in calcified turkey tendons and other substances are interpreted in terms of their structural anisotropy.

1. Introduction

The availability of X-ray area detectors at high-intensity synchrotron radiation sources has paved the way to conduct new exciting experiments for recording structural and textural changes on application of stress. We report here preliminary results of a study on turkey tendons. In turkey tendons one can, with the naked eye, see bundles of fibres organized in such a way that the fibre axes are generally parallel to the tendon axis.

At low magnifications ($\sim 30\times$), however, it becomes evident that the fibres are not completely parallel to the axis of the tendon but predominantly undulate in a zig-zag fashion to describe a periodicity in a range 10 to 100 μm. This morphology is known as crimps and exists generally in all the tissues (including human tissues) [1] which sustain tensile loading in life. It has been shown that crimps are functionally important because they are responsible for the nonlinear stress strain property of the fibres in the tissues such as tendons and ligaments. Briefly, at low-tensile loads zig-zag waveforms of the crimps open out. This gives rise to a relatively large deformation due to the opening out of the crimps. Once the crimps are straightened out, the fibre extension is governed according to the tensile compliance of the protein collagen itself. The changes in crimps in a bundle of collagenous fibres on application of stress can be detected by low-angle X-ray diffraction [2].

2. The area detector

The desirable characteristics of an ideal detector have been listed before [3]. The improved gas detector

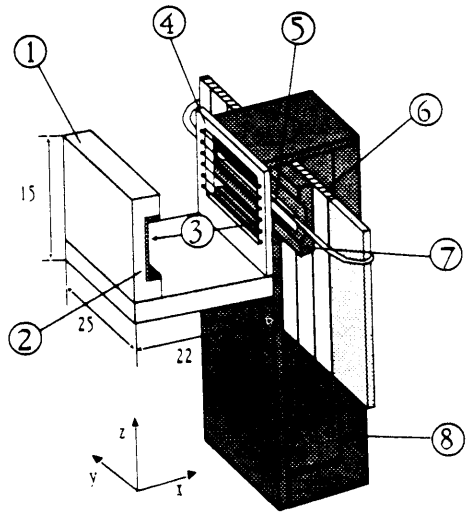

Fig. 1. Schematic construction geometry of the detector. (1) PVC frame, (2) drift field electrode (-3.0 kV), (3) drift region (17 mm), (4) grid wires ($+50$ V), (5) anode wire ($+1.6$ kV), (6) delay line (11 ns/mm), (7) semicylindrical cathode ($+50$ V), (8) cathode plate (ground potential).

Table 1
Performance of the drift chamber and the diffraction apparatus

Drift chamber:		
Quantum efficiency at $\lambda = 1.54$ Å and using Ar (Xe) mixtures	20 (84)	%
Detecting area	17×20	mm^2
Spatial resolution on the detector plane: X(drift) $\times$ Y(delay)	120×155	μm^2
Pixel number	142×125	pixels
Maximum storage of the buffer memories	256×256	pixels
Maximum counting rate for each pixel	2.2×10^4	cps
Maximum count capacity of the detector	1×10^6	cps
Maximum linear count of the whole system	7×10^5	cps
Diffraction apparatus:		
Diameter of the pinhole collimator (variable)	0.5	mm
Primary beam angular divergence: horizontal–vertical	76–6	arc sec
Cross section of the beam at the specimen: horizontal $\times$ vertical	0.68×0.51	mm^2
Intensity on the sample ($\lambda = 1.54$ Å, $\Delta\lambda/\lambda = 10^{-4}$, $I = 30$ mA single bunch)	2.4×10^7	photons/s
Conical angle of parasitic scattering	495	arc sec
Specimen–detector distance: maximum–minimum	500–40	mm
Maximum angle obscured by the beam stop	227	arc sec
Angular range covered by the detector at max. and min. distance	2–25	deg
Angle range covered by the goniometer at max. and min. distance	25–134	deg
Max. and min. angular resolution on the detector plane: X coordinate	50–618	arc sec
Max. and min. angular resolution on the detector plane: Y coordinate	66–825	arc sec

at Frascati, although not completely ideal, offers immunity from radiation damage, uniform sensitivity of detection, a wide dynamic range and high spatial resolution. The detector is interfaced to a real-time data acquisition system. The full characteristics of the detector are given in table 1. It should be noted that in

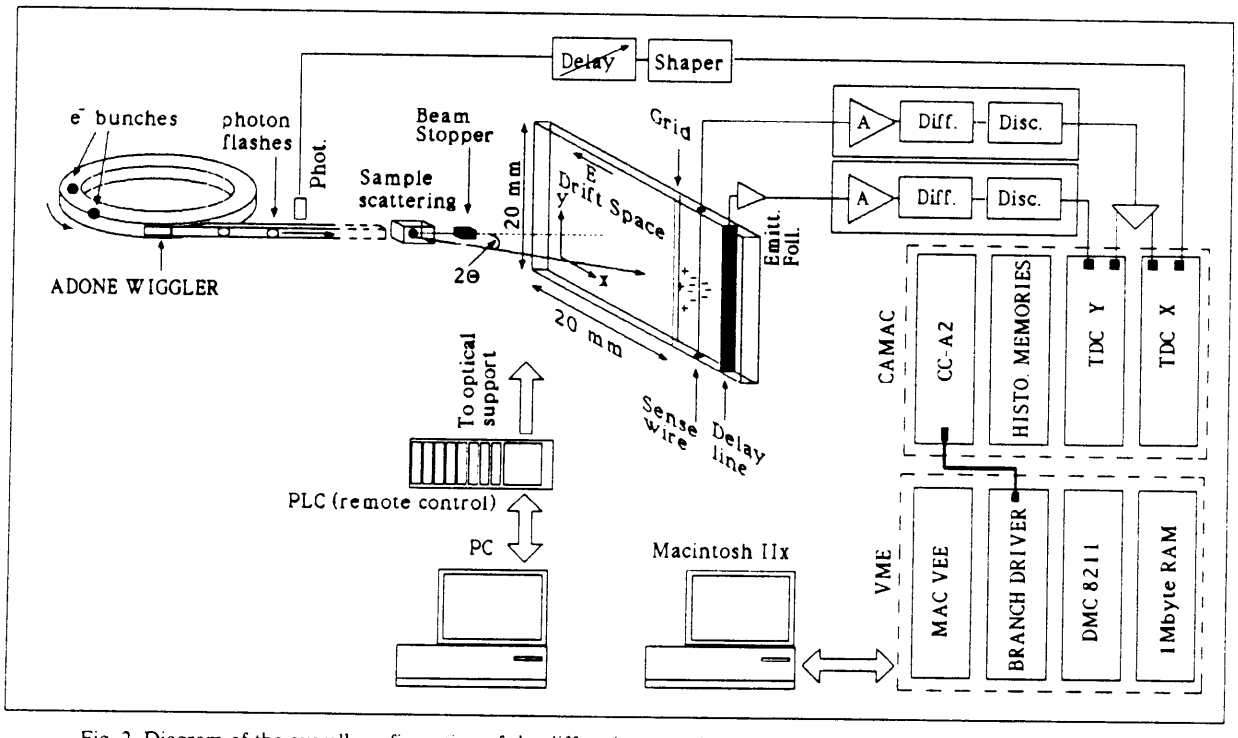

Fig. 2. Diagram of the overall configuration of the diffraction experiment with respect to the ADONE wiggler source.

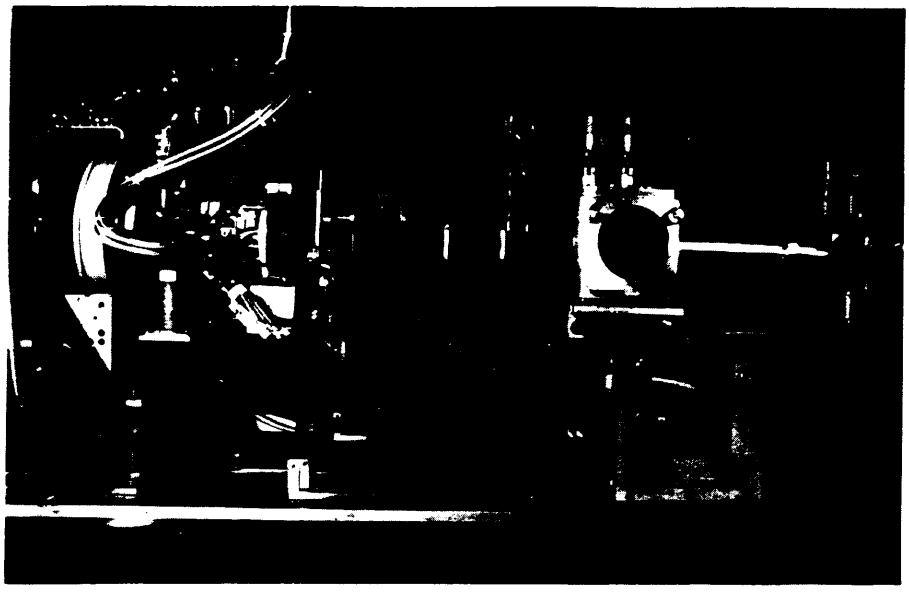

Fig. 3. Photograph of the diffraction apparatus with the drift-chamber area detector.

relation to other existing area detectors the maximum count rate is considerably improved to 0.7 MHz.

The construction geometry of the detector is schematically shown in fig. 1.

The x coordinate of a scattering event by an X-ray photon is determined by measuring drift time $\Delta t = t_1 - t_0$ of the electronic cloud, generated in the gas by the photon, which drifts in the detection plane at constant velocity up to the anode wire (t_0 is "the zero time" given by the time structure of the synchrotron radiation). The Y coordinate is measured by a delay line (11 ns/mm delay time), placed at a distance of 2.5 mm from the anode to detect the position of the avalanche discharge along the wire.

It should be noted that the performance of the detector has been improved because it has (a) no wire grid to produce a uniform electric potential detecting area, and (b) a small charge proportional gas gap region (2.5 mm), separated from the "drift region", where the high density of ion discharge avalanches can be easily collected by a semicylindrical cathode.

Further details of the mechanisms of operation can be found elsewhere [4]. The detector, mounted at 35 m from the ADONE wiggler source on a diffraction apparatus, is described below.

3. Diffraction apparatus

Fig. 2 shows the overall configuration of the diffraction apparatus and the rest of the system with respect to the ADONE wiggler source.

It has the same geometry as used previously [4]. Additionally we have incorporated an environmental chamber incorporating a fully automatic miniature tensometer for obtaining diffraction patterns of mechanically stretched, hydrated biological specimens [5]. There is also a thermostatic cell to hold a specimen in the temperature range -30 to $+150\,^{\circ}$C. It is possible to change the specimen–detector distance to obtain small-, medium- and wide-angle diffraction experiments on the same specimen because the detector is linked to the specimen chamber via a telescopic vacuum pipe.

During diffraction experiments parasitic scattering was considerably reduced by using a combination of 0.5 and 0.7 mm pinholes placed 500 mm apart. The relevant details of the other important parameters are given in table 1. For conducting spatial resolution tests pinholes of 110 and 200 μm diameter were used at a distance of 500 mm from each other. The apparatus also contains a beam-stop movable by remote control. It is placed on the entrance window of the detector. Fig. 3 shows a photograph of the assembled apparatus at the ADONE wiggler beam line. A fast remote control movement system (PLC Omron Sysmac C200H) for moving the whole apparatus and adjusting all the experimental parameters is available with the apparatus.

4. Data acquisition

To make full use of the area detector, a new fast data acquisition system, called ARGO (acquisition of data with Real-time Graphic Output) is available. This sys-

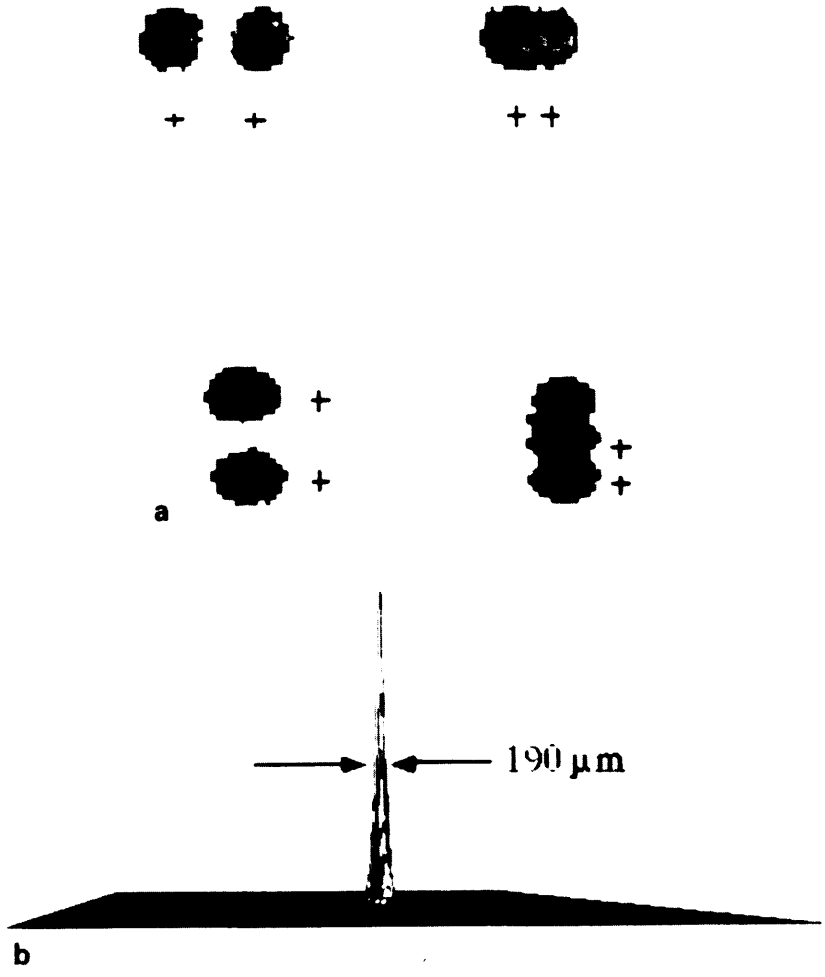

Fig. 4. Demonstration of the spatial resolution of the detector: (a) Spots on the top were recorded in the direction of the drift coordinate and those below in the direction of the delay line coordinate. The distance between the crosses on the left-hand side is 500 μm while that on the right is 250 μm. (b) Intensity profile of the beam passed through a pinhole of diameter 110 μm.

tem uses a Macintosh IIx computer to control CAMAC and the VME bus. The program for the system is in the Real-Time Fortran language (RTF), developed at CERN, in the "MacSys" system environment.

The functioning of the ARGO system can be better understood by referring to fig. 2. The output from a pair of LeCroy model 4204 CAMAC TDCs (time to digital converters), with conversion time of about 1 μs, is stored into two LeCroy 3588 histogram memories via a separate bus, independently of the CAMAC. During data taking, the histogram memories are read by a Macintosh computer through the VME subsystem [3] as shown in fig. 2. The Macintosh also displays the counts, graphically, obtained in 128 × 256 channels with a maximum of 65536 counts per channel or in 256 × 256 channels with a maximum of 4095 counts per channel, respectively. CAMAC commands also allow one to control TDC parameters and acquisition start–stop operations. It is possible to view different graphic displays of the experimental data in real time. One-dimensional projected intensity histograms (X or Y coordinate), two-dimensional pseudocolour plots, and two-dimensional intensity maps with the intensity displayed in the third dimensions can be viewed.

5. Resolution of the detector

To determine the spatial resolution of the detector, the primary beam was passed through a pinhole of 200 μm diameter. After obtaining sufficient counts the pinhole was moved in x and y directions by steps of

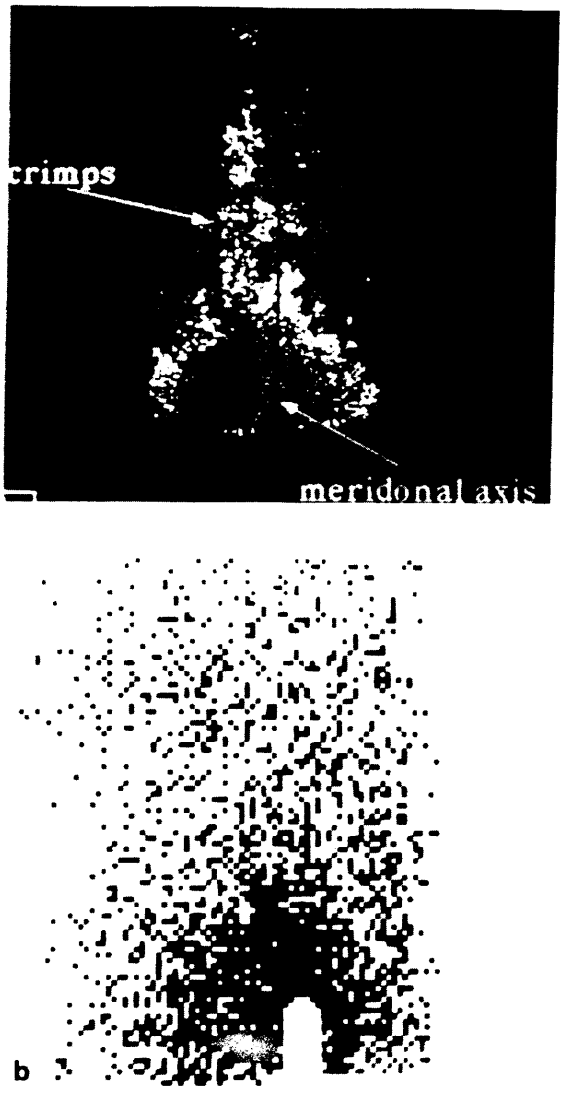

Fig. 5. Low-angle diffraction patterns of tendons from a 20-week-old turkey: (a) Unstretched uncalcified turkey tendon. The arrow shows the two reflections due to the presence of crimps overlapping along the apparatus meridional axis. (b) Stretched uncalcified turkey tendon showing the disappearance of the crimps.

250 and 500 μm. The new positions of the beam were recorded. These patterns are shown in fig. 4a. It is evident that the resolution of the detector is much better than 250 μm. This conclusion is further confirmed by fig. 4b, where the intensity profile of the beam passed through a pinhole of diameter 110 μm is shown. The half-width of the profile is 190 μm. The estimated resolution is therefore of the order of 155 μm.

6. Turkey tendon diffraction results

Figs. 5a and b show low-angle diffraction patterns of stretched and unstretched uncalcified turkey tendons.

Fig. 6. Continuous small-angle scattering intensity patterns from: (a) lupolen; (b) half-met hemocyanin from octopus; (c) calcified tendon from a 20-week-old turkey.

The diffraction pattern of the unstretched tendons clearly shows azimuthal split in the reflections originating from the 640 Å periodicity, confirming that there are two predominant meridional directions in the specimen, corresponding to the two directions of the crimp arms. In fact it is possible to measure the crimp angle from the intersection of the reflections. It is roughly 15° and matches well with the measurements by polarizing optical microscopy. The point of intersection of the reflections lies on the central axis of the detector and normal to the beam direction. This is also the direction which corresponds to the projection of the overall, nominal, axis of the fibres. It is evident in fig. 5b that on stretching the multiplicity of the meridional directions of the reflections disappears, confirming the fact that the crimps have straightened out on application of stress. A further point to note is that the unevenness of intensities of reflections around the nominal axial direction of the fibres may be due to the specimen tilt present with respect to the primary incident beam for both the specimens represented in figs. 5a and b.

7. Continuous small-angle scattering

Figs. 6a–c show continuous small-angle scattering intensity patterns from lupolen, half-met hemocyanin of octopus and calcified turkey tendon.

The patterns from these substances were used to confirm that the behaviour of the detector in the vicinity of the beam-stop is reliable. Measurements of the scattering vector in the reciprocal space for lupolen confirm that the dimension of the scattering units is 150 Å with an error of ±2 Å. The lupolen pattern also shows unevenness of the scattered intensity with respect to the meridional axis in the plane of the detector; the intensity on the left-hand side being slightly greater. Fig. 6b on the other hand shows that the scattering intensity for half-met hemocyanin has high intensity on the right-hand side of the meridian. Fig. 6c shows the continuous scattering pattern of a calcified tendon. This scattering is most probably due to the presence of hydroxyapatite. Deposition of hydroxyapatite in calcified tissues occurs in crystalline (hexagonal) form. The actual crystals are very small (~ 100 to 500 Å) and have a needle shape. The needles are generally aligned with the fibril/fibre axis. The continuous scattering pattern in fig. 6c is in accordance with the above facts. The discrete intensity spot in fig. 6c corresponds to the third-order reflection of the 640 Å periodicity of the collagen fibrils.

8. Conclusions

From this study it is evident that the spatial resolution of the improved drift chamber area detector at Frascati is extremely useful for studying low-angle diffraction and continuous small-angle scattering. Our experiments on calcified and uncalcified turkey tendons and those on lupolen and half-met hemocyanin have shown that the differences in intensity in both meridional and equatorial directions can be detected with ease. Uniformity of the spatial resolution throughout the plane of detection enables one to study effects such as azimuthal splitting and azimuthal spread with confidence. The data reported here is as yet not completely analyzed but it is clear that all the expected effects relating to anisotropy of scattering units can be studied. With high-photon-flux beams it should be possible to record changes in diffraction and scattering dynamically in real time.

Acknowledgements

We thank the group of Prof. A. Congiu-Castellano of "La Sapienza" University of Rome for providing some specimens, Mr. M. Brolatti of ISM-CNR of Frascati for designs, the PWA group of INFN for the provision of the ADONE wiggler beam line, "Gruppo V" of INFN for financial support for the development of the ARGO system under the FADD research grant and the EEC for the financial support for the work on turkey tendons.

References

[1] J.S. Shah, W.G.J. Hempson and M.I. Jayson, Eng. in Medicine 8 (1979) 1.
[2] S.P. Nicholls, L.J. Gathercole and J.S. Shah, Ann. Rheum. Dis. 43 (1984) 477.
[3] A. La Monaca, E. Burattini, G. Cappuccio, J.S. Shah, S. Simeoni, A. Stecchi and L. Trasatti, Proc. 2nd Eur. Conf. on Progress in X-ray Synchrotron Radiation Research, Rome, 1989, eds. A. Balerna, E. Bernieri and S. Mobilio, Conf. Proc. vol. 25 (Italian Physical Society, Bologna, 1990) p. 345.
[4] M. Iannuzzi and A. La Monaca, Nucl. Instr. and Meth. 201 (1982) 197.
[5] J.S. Shah, A. La Monaca, A. Stecchi, L. Trasatti and E. Burattini, ref. [3], p. 433.